J|A|C|S ARTICLES

Published on Web 02/04/2009

Photocurrent Enhancement of n-Type Cu_2O Electrodes Achieved by Controlling Dendritic Branching Growth

Colleen M. McShane and Kyoung-Shin Choi*

Department of Chemistry, Purdue University, West Lafayette, Indiana 47907

Received August 11, 2008; E-mail: kchoi1@purdue.edu

Abstract: Cu_2O electrodes composed of dendritic crystals were produced electrochemically using a slightly acidic medium (pH 4.9) containing acetate buffer. The buffer played a key role for stabilizing dendritic branching growth as a pH drop during the synthesis prevents formation of morphologically unstable branches and promotes faceted growth. Dendritic branching growth enabled facile coverage of the substrate with Cu_2O while avoiding growth of a thicker Cu_2O layer and increasing surface areas. The resulting electrodes showed n-type behavior by generating anodic photocurrent without applying an external bias (zero-bias photocurrent under short-circuit condition) in an Ar-purged 0.02 M K_2SO_4 solution. The zero-bias photocurrent of crystalline dendritic electrodes was significantly higher than that of the electrodes containing micrometer-size faceted crystals deposited without buffer. In order to enhance photocurrent further a strategy of improving charge-transport properties by increasing dendritic crystal domain size was investigated. Systematic changes in nucleation density and size of the dendritic Cu_2O crystals were achieved by altering the deposition potential, Cu^{2+} concentration, and acetate concentration. Increasing dendritic crystal size consistently resulted in the improvement of photocurrent regardless of the method used to regulate crystal size. The electrode composed of dendritic crystals with the lateral dimension of ca. 12000 μm^2 showed more than 20 times higher zero-bias photocurrent than that composed of dendritic crystals with the lateral dimension of ca. 100 μm^2. The n-type nature of the Cu_2O electrodes prepared by this study were confirmed by linear sweep voltammetry with chopped light and capacitance measurements (i.e., Mott−Schottky plots). The flatband potential in a 0.2 M K_2SO_4 solution (pH 6) was estimated to be −0.78 vs Ag/AgCl reference electrode. The IPCE measured without applying an external bias was approximately 1% for the visible region. With appropriate doping studies and surface treatment to improve charge transport and interfacial kinetics more efficient n-type Cu_2O electrodes will be prepared for use in various photoelectrochemical and photovoltaic devices.

Introduction

Cuprous oxide (Cu_2O) is a direct band-gap semiconductor highly desirable for use in solar energy conversion due to its band gap (E_g = 1.9−2.2 eV) and relatively high absorption coefficient in the visible region.[1−7] The conduction band and valence band of Cu_2O are located near the reduction and oxidation potentials of water, respectively. As a result, Cu_2O is also a viable candidate to produce hydrogen by direct water photolysis using visible light with little or no external bias.[8−10] The low cost and environmentally benign nature of copper makes developing Cu_2O-based photoelectrochemical cells more attractive.

Cu_2O is typically prepared as a p-type material due to the presence of copper vacancies.[1] Only a handful of synthesis conditions to prepare n-type Cu_2O have been reported to date.[11−17] Developing a facile and practical method to produce highly photoactive n-type Cu_2O electrodes can be beneficial as it will allow for building solar cells or photoelectrochemical cells based on a p−n Cu_2O homojunction which is predicted to achieve a higher efficiency than heterojunction solar cells constructed with p-type Cu_2O.[5] It will also generate new

(1) Rakhshani, A. E. *Solid-State Electron.* **1986**, *29*, 7–32.
(2) Akimoto, K.; Ishizuka, S.; Yanagita, M.; Nawa, Y.; Paul, G. K.; Sakuri, T. *Sol. Energy* **2006**, *80*, 715–722.
(3) Rai, B. P. *Sol. Cells* **1988**, *25*, 265–272.
(4) Musa, A. O.; Akomolafe, T.; Carter, M. J. *Sol. Energy Mater. Sol. C.* **1998**, *51*, 305–316.
(5) Olsen, L. C.; Addis, F. W.; Miller, W. *Sol. Cells* **19821983**, *7*, 247–279.
(6) Izaki, M.; Shinagawa, T.; Mizuno, K.-T.; Ida, Y.; Inaba, M.; Tasaka, A. *J. Phys. D: Appl. Phys.* **2007**, *40*, 3326–3329.
(7) Mittiga, A.; Salza, E.; Sarto, F.; Tucci, M.; Vasanthi, R. *Appl. Phys. Lett.* **2006**, *88*, 163502.
(8) Hara, M.; Kondo, T.; Komoda, M.; Ikeda, S.; Shinohara, K.; Tanaka, A.; Kondo, J. N.; Domen, K. *Chem. Commun.* **1998**, 357–362.
(9) de Jongh, P. E.; Vanmaekelbergh, D.; Kelly, J. J. *Chem Commun.* **1999**, 1069–1070.
(10) Nian, J.-N.; Hu, C.-C.; Teng, H. *Int. J. Hydrogen Energy* **2008**, *33*, 2897–2903.
(11) Siripala, W.; Jayakody, J. R. P. *Sol. Energy Mater.* **1986**, *14*, 23–27.
(12) Wijesundara, R. P.; Perera, L. D. R. D.; Jayasuriya, K. D.; Siripala, W.; DeSilva, K. T. L.; Samantilleke, A. P.; Dharmadasa, I. M. *Sol. Energy Mater. Sol. C.* **2000**, *61*, 277–286.
(13) Garuthara, R.; Siripala, W. *J. Lumin.* **2006**, *121*, 173–178.
(14) Fernando, C. A. N.; Bandara, T. M. W. J.; Wethasingha, S. K. *Sol. Energy Mater.* **2001**, *70*, 121–129.
(15) Fernando, C. A. N.; de Silva, P. H. C.; Wethasingha, S. K.; Dharmadasa, I. M.; Delsol, T.; Simmonds, M. C. *Renewable Energy* **2002**, *26*, 521–529.
(16) Balamurugan, B.; Aruna, I.; Mehta, B. R.; Shivaprasad, S. M. *Phys. Rev.* **2004**, *B69*, 165419.
(17) Wang, L.; Tao, M. *Electrochem. Solid-State Lett.* **2007**, *10*, H248−H250.

 © 2009 American Chemical Society

Scheme 1. Increasing Surface Areas of the Electrode by (a) Increasing Nucleation Density while Reducing Crystal Sizes and (b) Inducing Dendritic Branching Growth without Increasing Nucleation Density; (c) Electrode Composed of One Dendritic Crystal Covering the Entire Substrate[a]

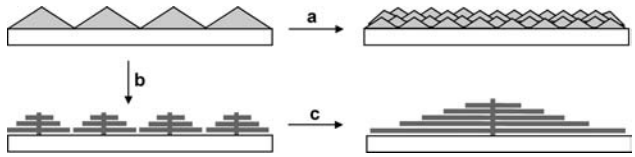

[a] This electrode may achieve both high surface areas and excellent charge-transport properties.

opportunities to assemble various heterojunction photoelectrodes based on n-type Cu_2O electrodes.

In this study, we report the synthesis condition to electrochemically prepare high-performance n-type Cu_2O photoelectrodes using a slightly acidic aqueous medium (pH 4.9). The unique focus of this study lies in investigating a new strategy of enhancing the photocurrent of polycrystalline n-type Cu_2O electrodes via rational morphology control. More specifically, we investigate exploiting and regulating dendritic growth of Cu_2O as a means to simultaneously achieve high surface areas and good electrical continuity within the electrodes. For typical polycrystalline electrodes, increasing surface areas (i.e., electrode/electrolyte interfacial areas) involves making particles smaller (i.e., nanocrystalline electrodes), which results in equally enhanced particle−particle interfacial areas, significantly decreasing charge-transport properties (Scheme 1a). However, dendritic growth allows for increasing surface areas without increasing nucleation density by forming multiple branches from a single nucleus (Scheme 1b). As these branches grow forming a physically continuous crystal body, excellent charge-transport properties are expected within the dendritic crystal. If the nucleation density, crystal domain size, and degree of dendritic branching can be methodically controlled, an optimum combination of surface area and charge-transport properties may be achieved. Scheme 1c shows an electrode composed of one dendritic crystal with the branches covering the entire substrate. This electrode can be considered a single-crystalline electrode in the sense that the whole electrode is developed from a single nucleus and that the atomic level continuity of a crystal structure is present throughout the entire electrode. At the same time, due to the presence of complex branching patterns it can achieve higher surface areas and surface reactivities than typical single-crystalline electrodes.

Electrodeposition of Cu_2O involves two steps: reduction of Cu^{2+} ions to Cu^+ ions (eq 1) and precipitation of Cu^+ ions to Cu_2O due to the solubility limitation of Cu^+ ions (eq 2).[18]

$$Cu^{2+} + e^- \leftrightarrow Cu^+ \quad E^o = 0.159\ V \tag{1}$$

$$2Cu^+ + H_2O \leftrightarrow Cu_2O + 2H^+ \quad \log[Cu^+] = 0.84 - pH \tag{2}$$

$$2Cu^{2+} + H_2O + 2e^- \leftrightarrow Cu_2O + 2H^+ \ \text{(overall reaction)}$$

Generally speaking, the dendritic branching growth in electrodeposition can be induced when the deposition rate is increased to form a depletion zone of the nutrient ions (i.e., Cu^{2+} for Cu_2O deposition) around a growing crystal.[19,20] Once the depletion zone is formed, the apexes of a polyhedral crystal, which protrude into the region of higher concentration, grow faster than the central parts of facets; thus, dendritic branches are formed (mass-transport-limited growth).[20−22] The difficulty of stabilizing the dendritic growth of Cu_2O lies in the fact that H^+ is produced as the side product of Cu_2O deposition (eq 2). As the deposition rate of Cu_2O increases, the local pH at the working electrode decreases simultaneously. A decrease in pH increases the solubility of Cu^+ ions and therefore the reversibility of Cu_2O crystallization (eq 2). Under this condition, thermodynamically unstable morphologies (i.e., branches) cannot be formed or maintained as they can transform into energetically more stable faceted morphologies by the dissolution and reprecipitation processes.[23] Another difficulty of stabilizing dendritic Cu_2O crystals is that the deposition potential or current cannot be increased unlimitedly because of the possibility of reducing Cu^{2+} ions to Cu metal.

In order to overcome these difficulties and induce the dendritic growth of Cu_2O we exploited buffered plating media that can keep the pH near the working electrode constant regardless of the deposition rate.[23] Here, we describe methods to produce and manipulate dendritic n-type Cu_2O electrodes and discuss the effect of morphological features on photocurrent generation. The dendritic Cu_2O electrodes produced in this study show a considerable amount of zero-bias photocurrent (photocurrent generated without application of an external bias) that varies significantly upon dendritic morphology tuning. To the best of our knowledge, n-type Cu_2O electrodes generating zero-bias photocurrent for the photoelectrolysis of water without the use of additional electron- or hole-accepting species (e.g., O_2, formate) have not been reported previously. This study will provide new insight into tuning morphologies for the enhancement of desired properties of polycrystalline electrodes as well as opportunities to build various photoelectrochemical devices based on high-performance n-type Cu_2O electrodes.

Experimental Section

Materials. Copper(II) acetate ($Cu(OOCCH_3)_2 \cdot H_2O$, 98−102% purity), copper(II) nitrate trihydrate ($Cu(NO_3)_2 \cdot 3H_2O$), and acetic acid (CH_3COOH, 80+% purity) were obtained from Alfa Aesar, Acros Organics, and Mallinckrodt, respectively, and used as purchased. Copper(II) sulfate anhydrous ($CuSO_4$, ≥99% purity) and lactic acid ($CH_3CH(OH)CO_2H$, 85+% solution in water) were purchased from Sigma-Aldrich, and sodium hydroxide (NaOH, 99% purity) was purchased from Mallinckrodt. All were used as purchased. The solutions used in this work were prepared with DI water further purified with a Millipore Milli-Q purification system (resistivity ≥ 18.2 MΩ).

Electrodeposition of Cu_2O Electrodes. A standard three-electrode setup in an undivided cell was used (Princeton Applied Research VMP2 Multichannel Potentiostat/Galvanostat). Indium-doped tin oxide (ITO) (8−12 Ω resistance) was used as the working electrode. The counter electrode consisted of 1000 Å of platinum deposited on 300 Å of titanium on a glass slide by electron beam evaporation. The reference electrode was an Ag/AgCl electrode in 4 M KCl solution, against which all potentials reported herein were measured.

Cuprous oxide electrodes composed of faceted cubic crystals were electrodeposited from an 0.02 M $Cu(NO_3)_2$ aqueous solution using a constant potential of +0.02 V. The temperature of the deposition bath was maintained at 60 °C.

(18) Pourbaix, M. *Atlas of Electrochemical Equilibria in Aqueous Solutions*, 2nd English ed.; National Association of Corrosion Engineers: Houston, 1974; pp 384−392.
(19) Brady, R. M.; Ball, R. C. *Nature* **1984**, *309*, 225–229.
(20) López, C. M.; Choi, K.-S. *Langmuir* **2006**, *22*, 10625–10629.
(21) Berg, W. F. *Proc. R. Soc.* **1938**, *A164*, 79–96.
(22) Yokoyama, E.; Kudora, T. *Phys. Rev.* **1990**, *A41*, 2038–2049.
(23) Siegfried, M. J.; Choi, K.-S. *Angew. Chem., Int. Ed.* **2008**, *47*, 368–372.

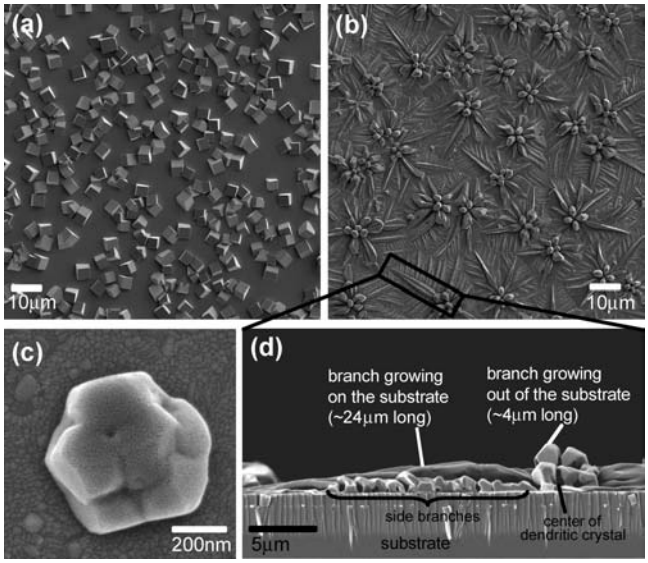

Figure 1. SEM images of Cu_2O deposited at $E = 0.02$ V using a solution containing (a) 0.02 M $Cu(NO_3)_2$ and (b) 0.02 M $Cu(CH_3COO)_2$ and 0.08 M acetate buffer (pH 4.9). (c) SEM image of a dendritic crystal at an early stage showing a truncated octahedral morphology, and (d) the side-view SEM image of a dendritic crystal showing anisotropic branch development.

Cuprous oxide electrodes composed of dendritic crystals were electrodeposited from aqueous solutions containing 0.005−0.02 M $Cu(CH_3COO)_2$ and acetic acid buffers. Buffered solutions were prepared by dissolving a desired quantity of acetic acid in a plating solution and adding sodium hydroxide until the pH reached 4.9. The concentrations of buffer reported in this study do not include acetate ions from $Cu(CH_3COO)_2$. The deposition bath was maintained at a temperature of 70 °C while a constant potential of 0.0, +0.02, or +0.06 V was applied to the system. Deposition was continued until the ITO substrate was completely covered with Cu_2O, which can be monitored by the change in deposition current: the current density drops below ca. −0.015 mA/cm^2. (Typical deposition current density maximums range from approximately −0.5 to −1.25 mA/cm^2.) It typically takes 15−95 min of deposition depending on the applied potential and compositions of the plating solutions.

For comparison purposes (see Supporting Information), p-type Cu_2O films were electrodeposited from aqueous solutions containing 0.4 M $CuSO_4$ and 3 M lactic acid. Prior to deposition the solutions were brought to pH 11 through addition of sodium hydroxide. The deposition media was kept at a temperature of 60 °C, and a potential of −0.4 V was applied for 30 min.[24,25]

After each deposition the resulting film was thoroughly rinsed with deionized water and dried with a gentle stream of nitrogen gas.

Characterization. X-ray diffraction (XRD) patterns were recorded on a Scintag X2 diffractometer (Cu Kα radiation). Scanning electron microscopy (SEM) images were obtained using a JEOL JSM-840 scanning electron microscope operated at 5 kV. The films were coated with Au and Pd by thermal evaporation before imaging to minimize charging problems. In the case of Figure 1c and the inset of Figure 9b a FEI Nova NanoSEM 200 operated at 5 kV was utilized. In order to take side-view images, Cu_2O electrodes were cut and a portion was mounted on the sample holder such that the side of the sample was perpendicular to the electron beam. UV−vis absorption spectra were obtained using a diffuse reflectance mode by a Varian Cary 300 Bio UV−visible Spectrometer. Samples for diffuse reflectance measurement were prepared by scratching Cu_2O powders off the ITO substrate, pulverizing them with a mortar and pestle, and spreading them into packed barium sulfate powder that was used as a reference to collect a background spectrum.

Photoelectrochemical and Electrochemical Measurements. The zero-bias photocurrent reported in this study was obtained without applying an external bias between the Cu_2O electrode and the counter electrode (short-circuit condition). A platinum electrode (1000 Å of platinum deposited on 300 Å of titanium on a glass slide by electron beam evaporation) was used as the counter electrode. The deposited Cu_2O electrodes were set to face an optical fiber leading from a 300 W xenon arc lamp containing a UV filter. The spot size and intensity of the light that came out of the optical fiber (with the UV filter in place) were 0.1 cm^2 and 1 W/cm^2, respectively. A 0.02 M potassium sulfate (K_2SO_4, 99% purity, purchased from Mallinckrodt) solution was used for photocurrent measurements. Prior to measurements, the solutions were purged of O_2 through the bubbling of Ar for at least 30 min. When O_2 is present, reduction of O_2 is a thermodynamically more feasible photoreduction reaction than production of H_2. Therefore, in order to probe whether the Cu_2O electrodes have the proper energetics to produce H_2, removal of other electrochemically active species is necessary.

For linear sweep voltammetry (LSV) of the Cu_2O electrodes, potential was scanned from 0.2 to −1.0 V with a scan rate of 20 mV/s in an Ar-purged 0.2 M K_2SO_4 solution while being irradiated with chopped light (1 Hz) using a 300 W xenon arc lamp (light intensity, 100 mW/cm^2). Photocurrent action spectra (i.e., incident photon to current conversion efficiency (IPCE) vs excitation wavelength) were obtained in an Ar-purged 0.2 M K_2SO_4 solution under short-circuit condition using light from a 300 W Xe lamp passing through an AM1.5 global filter (Newport Corp. 81094), a monochromator (Newport Corp. CS 130 1/8m, bandwidth 4 nm), and the fiber optic bundle. The light intensity exiting the fiber optic bundle was measured with a Si photodiode (Oriel 71580). Capacitance measurements were carried out to obtain Mott−Schottky plots using an EG&G Princeton Applied Research Potentiostat/Galvanostat model 263A interlinked with a Princeton Applied Research FRD100 frequency response detector. A standard three-electrode setup described previously was used with a Cu_2O electrode as the

Scheme 2. (a) Anisotropic Lateral Growth of Faceted Crystals Results in Creating High Index Planes That Are Thermodynamically Unstable, while (b) That of Dendritic Crystals Does Not Result in an Additional Increase in Surface Energy As It Does Not Involve Formation of Higher Index Planes

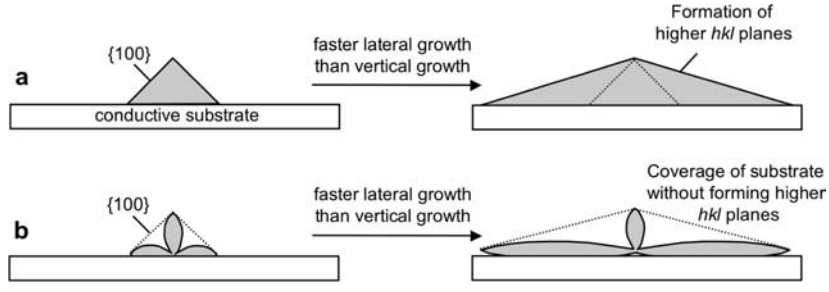

working electrode in an Ar-purged 0.2 M K_2SO_4 solution. A sinusoidal perturbation of 10 mV was applied at a frequency of 10 kHz.

Results and Discussions

Figure 1a shows typical SEM images of cubic Cu_2O crystals deposited on a ITO substrate when an unbuffered plating solution containing 0.02 M $Cu(NO_3)_2$ was used. In this medium, no sign of dendritic growth was observed even when the applied potential was increased to a point that triggers deposition of copper metal. This indicates that stabilizing dendritic growth of pure Cu_2O is not possible in this medium. We postulated that in an unbuffered medium branching growth may not occur even if mass-transport-limited growth conditions are created because the significant pH drop at the working electrode, caused by H^+ production during Cu_2O deposition (eq 2), can hinder formation of morphologically unstable branches as we discussed in the Introduction. The effect of H^+ ions on promoting faceted growth and suppressing branching growth was published elsewhere.[23] To test this supposition we introduced an acetate buffer to the plating medium and repeated depositions. Acetate buffer was chosen because it is electrochemically inert under the deposition conditions we used, and its pK_a value (4.74) is close to the pH of the freshly prepared plating solution used to deposit Cu_2O cubes.

When deposition was carried out at $E = 0.02$ V using a 0.02 M $Cu(CH_3COO)_2$ solution containing 0.08 M acetate buffer (pH 4.9) Cu_2O was deposited as dendritic crystals (Figure 1b). This result indicates that the initial deposition rate achieved by $E = 0.02$ V is enough to induce the mass-transport-limited growth, but it was the local pH drop at the working electrode in an unbuffered medium that suppressed formation of branched Cu_2O crystals. The dendritic crystals obtained in a buffered medium do not possess cubic shapes judging from the number and positions of the branches (the tips of the branches are developed from the apexes of a polyhedron). An SEM image captured at an early statge of dendritic growth confirms that the dendritic crystals are developed from truncated octahedral crystals (Figure 1c). The shape change from cubic to truncated octahedral is due to the acetate ions in the buffer preferentially adsorbing {111} planes slowing down crystal growth along the ⟨111⟩ directions. This results in some portions of {111} planes remaining in the final morphology, converting a cubic shape to a truncated octahedral shape.[26]

Another feature to notice in Cu_2O dendritic growth is their anisotropic development of branches. Figure 1b and 1d shows that the branches grown on the substrate are significantly longer than the branches grown out of the substrate, although all main branches (branches developed from the apexes of a polyhedron) are symmetrically equivalent for Cu_2O structure (space group no. 224, $Pn\bar{3}m$). This is because the ITO substrate is much more conductive than Cu_2O crystals, making branches on the substrate grow faster than those growing out of the substrate. (More Cu^+ ions are produced on the ITO surface than on the tips of Cu_2O branches growing out of the substrate.) When Cu_2O grows as faceted crystals lateral growth being faster than vertical growth would result in exposing thermodynamically unstable high index surfaces, which is unfavorable regardless of the difference in conductivity of ITO and Cu_2O (Scheme 2a). For dendritic growth that does not involve formation of flat facets asymmetric development of branches does not result in an additional increase in surface energy and can occur if it is kinetically feasible (Scheme 2b). From a practical point of view, this anisotropic growth of dendritic crystals is highly advantageous as it allows for facile coverage of the substrate without equivalent vertical growth, minimizing the film thickness.

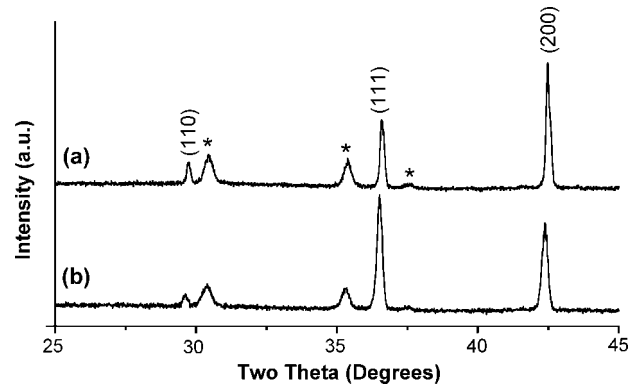

Figure 2. XRD of Cu_2O electrodes composed of (a) faceted and (b) dendritic crystals. Peaks generated by the ITO substrate are indicated by an asterisk (*).

The XRD patterns of the electrodes composed of faceted and branched crystals show that both Cu_2O electrodes are highly crystalline without needing a postdeposition annealing procedure (Figure 2). No impurity peaks from copper metal or CuO are present in these patterns.

The effect of the dendritic morphology on the photoelectrochemical properties was investigated by comparing the zero-bias photocurrent (short-circuit condition) of the electrodes composed of faceted and dendritic crystals. The electrodes used for this measurement were prepared by passing the same amount of charge ($Q = 0.175$ mAh cm^{-2}) during deposition to ensure that they contain the identical amount of Cu_2O deposits. A 0.02 M K_2SO_4 solution was used as an electrolyte and purged with Ar to eliminate dissolved O_2 prior to photocurrent measurement. As a result, the electrolyte did not contain any redox species that can be photoelectrochemically reduced or oxidized other than H^+, OH^-, and H_2O. Only visible light was used for the photocurrent measurement, using an UV-filter, to demonstrate Cu_2O's utilization of visible light to generate photocurrent.

Both faceted and dendritic Cu_2O electrodes generated anodic photocurrent upon illumination, which is an n-type behavior (Figure 3). This indicates that an upward band bending is formed at the Cu_2O/electrolyte junction and photon-generated holes are consumed at the Cu_2O/electrolyte interface to oxidize water.[27,28] The photon-generated electrons are transferred to the platinum counter electrode and then used to reduce water. After an initial anodic current spike the faceted Cu_2O electrode showed negligible steady-state photocurrent (<1 μA) due to the limited surface area provided by micrometer-sized cubes (Figure 3a). Compared to this value, the dendritic Cu_2O electrode shows a considerably enhanced photocurrent (steady-state photocurrent $= 0.06$ mA cm^{-2}), indicating that the dendritic branching morphology efficiently increased surface coverage and surface areas (Figure 3b). Cu_2O electrodes that are electrodeposited using an alkaline lactate medium, which has been a conventional

(24) Golden, T. D.; Shumsky, M. G.; Zhou, Y. C.; VanderWerf, R. A.; VanLeeuwen, R. A.; Switzer, J. A. *Chem. Mater.* **1996**, *8*, 2499–2504.
(25) Zhou, Y. C.; Switzer, J. A. *Mater. Res. Innovations* **1998**, *2*, 22–27.
(26) Siegfried, M. J.; Choi, K.-S. *Adv. Mater.* **2004**, *16*, 1743–1746.
(27) Nozik, A. J. *Annu. Rev. Phys. Chem.* **1978**, *29*, 189–222.
(28) Bak, T.; Nowotny, J.; Rekas, M.; Sorrell, C. C. *Int. J. Hydrogen Energy* **2002**, *27*, 991–1022.

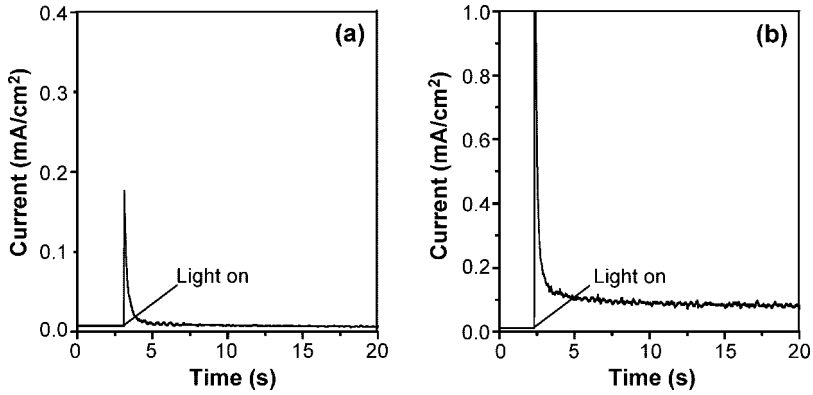

Figure 3. Zero-bias photocurrent of Cu_2O electrodes composed of (a) faceted cubic crystals and (b) dendritic crystals measured in a 0.02 M K_2SO_4 solution under 1 W/cm^2 illumination.

medium to electrodeposit Cu_2O,[24,25,29] show p-type behavior and do not generate noticeable zero-bias photocurrent under our experimental conditions (see Supporting Information).[9] Thus, the zero-bias photocurrent observed in this study is exciting not only for the direction (anodic vs cathodic photocurrent) but also for the magnitude.

In order to probe the possibility of further optimizing morphology for photocurrent enhancement we investigated synthesis conditions to decrease nucleation densities and increase domain size of dendritic crystals. Our intention was to improve the electrical continuity within the polycrystalline electrodes and reduce recombination losses by increasing the size of domains, which have a nature similar to single crystals, and decreasing crystal−crystal boundary areas. For typical faceted crystals decreasing nucleation density is not desirable as it results in a significant decrease in surface areas and an increase in electrode thickness as fewer crystals are grown larger in order to achieve a full coverage of the substrate. For polycrystalline Cu_2O electrodes having a high absorption coefficient and a high resistivity growing a thicker layer is disadvantageous for photocurrent enhancement.[1,3] However, for dendritic growth stabilized in this study a decrease in nucleation density may not result in a significant increase in film thickness owing to its tendency to develop branches in an asymmetric fashion (Scheme 2b). In addition, a decrease in surface area caused by reducing nucleation density may be less severe in dendritic growth because larger dendritic crystals can still achieve high surface areas by creating complex side branches from the main branches. Therefore, increasing the crystal domain size in dendritic branching growth may allow for improving charge-transport properties without losing too much surface area, thus improving photocurrent generation.

We observed that nucleation of Cu_2O under our deposition condition is instantaneous, meaning that the nucleation process occurs only at the early stage of deposition.[30] For the remaining deposition period the existing nuclei grow uniformly without forming new nuclei. The narrow size distribution observed for the crystals shown in Figure 1a is a good indication of instantaneous nucleation. We also observed that nucleation of Cu_2O occurs predominantly on the ITO substrate and not on top of the growing Cu_2O crystals. This nucleation behavior

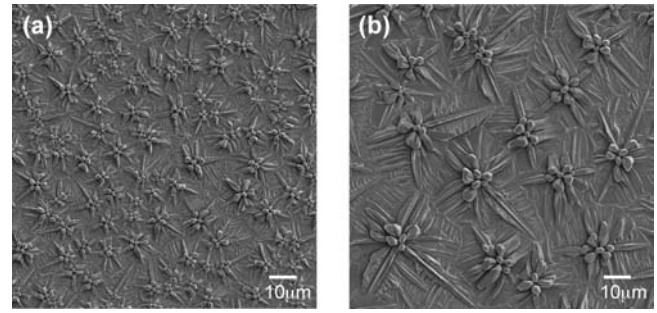

Figure 4. SEM images of dendritic Cu_2O electrodes obtained at E = (a) 0.00 (sample 1) and (b) 0.06 V (sample 3) using a solution containing 0.02 M $Cu(CH_3COO)_2$ M and 0.08 M acetate buffer (pH 4.9).

enables us to change crystal domain size by altering the initial nucleation density and letting the deposition continue until the substrate is completely covered with Cu_2O. Once complete, the final average crystal size should be inversely proportional to the number of nuclei.

One straightforward method to decrease the nucleation density in dendritic Cu_2O electrode is to decrease the deposition overpotential (η), which is defined as the difference between the applied deposition potential (E_{appl}) and the reduction potential of Cu^{2+} to Cu^{+} (E_{red}). For cathodic deposition, η increases as E_{appl} shifts to the more negative direction.

$$\eta = |E_{appl} - E_{red}| \tag{3}$$

$$E_{red} = E^{o} - 0.05916 \log([Cu^{+}]/[Cu^{2+}]) \text{ at } T = 298.15 \text{ K} \tag{4}$$

Figure 4 shows SEM images of Cu_2O electrodes nucleation density that were altered by varying E_{appl} (E_{appl} = 0.00 and 0.06 V). For each condition, deposition was continued until the substrate was completely covered with Cu_2O. The Cu_2O electrode deposited at 0.00 V (sample 1, Figure 4a) shows a significant increase in nucleation density compared to that deposited at E = 0.02 V (sample 2, Figure 1b) due to the increase in η. The lateral size of the crystals decreased accordingly from ca. 500 (sample 2) to ca. 100 μm^2 (sample 1). The opposite phenomenon was observed for the electrode deposited at E = 0.06 V (sample 3, Figure 4b); the nucleation density is decreased, and the lateral crystal size is increased to ca. 700 μm^2.

The comparison of the zero-bias photocurrent of samples 1−3 is shown in Figure 5a. The steady-state photocurrent gradually increases as the crystal size increases, although an increase in

(29) Mizuno, K.; Izaki, M.; Murase, K.; Shinagawa, T.; Chigane, M.; Onaba, M.; Tasaka, A.; Awakura, Y. *J. Electrochem. Soc.* **2005**, *152*, C179-C182.
(30) Paunovic, M.; Schlesinger, M. *Fundamentals of Electrochemical Deposition*; John Wiley & Sons, Inc.: New York, 1998, p 109.

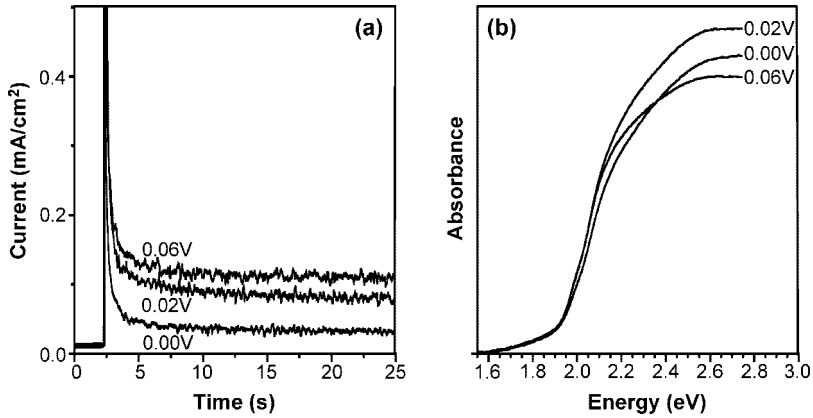

Figure 5. (a) Zero-bias photocurrent measured in a 0.02 M K_2SO_4 solution under 1 W/cm^2 illumination, and (b) UV−vis spectra of dendritic Cu_2O electrodes deposited at $E = 0.00$ (sample 1), 0.02 (sample 2), and 0.06 V (sample 3).

crystal size resulted in a decrease in surface areas judging from the SEM images. This means that the advantage gained by increasing crystal size (i.e., reduced recombination at the crystal boundary areas, electrical continuity in larger domains) is more significant than the disadvantage caused by reduction of Cu_2O/electrolyte interfacial areas in our dendritic Cu_2O system. Sample 3, possessing the largest dendritic crystals, shows 4.5 times higher steady-state photocurrent (0.09 mA/cm^2) than sample 1, which possesses the smallest crystal size (0.02 mA/cm^2).

The XRD patterns of samples 1−3 are identical and composed of only pure Cu_2O peaks (data not shown), confirming that the observed difference in photocurrent is not due to compositional changes caused by using different deposition potentials to prepare these electrodes. The UV−vis spectra of these electrodes also show identical absorption features (i.e., onset of band-gap transition and pre-band-gap transition structures) (Figure 5b), suggesting that the photocurrent difference is originated only from morphological differences of samples 1−3. However, in order to exclude the possibility that the observed changes in photocurrent are caused by less evident compositional changes caused by varying deposition potentials (e.g., doping, defects), which may not be detected by XRD or UV−vis spectra, it is necessary to alter the nucleation density and crystal size of Cu_2O by means other than applied potential. If the same trend is observed, we can conclude that the crystal domain size is truly the main factor that governs the photocurrent generation in our Cu_2O system.

The primary factor affecting the nucleation density of electrodeposition is η. Equation 3 shows that η depends not only on E_{appl} but also on E_{red}. E_{red} can be altered by the concentration of Cu^{2+} as shown in the Nernst equation (eq 4). Therefore, a systematic change in nucleation density and dendritic crystal size can be achieved by changing the concentration of Cu^{2+} ions in the plating solution while using a fixed E_{appl}. SEM images of dendritic Cu_2O electrodes deposited with $[Cu^{2+}] = 0.01$ (sample 4) and 0.005 M (sample 5) are shown in Figure 6. As the Cu^{2+} concentration decreases, E_{red} shifts to the more negative direction, thus decreasing η when E_{appl} is constant ($E_{appl} = 0.02$ V). This results in a decrease in nucleation density and an increase in crystal size. The average lateral crystal size of sample 5 (2000 μm^2) is approximately four times larger than that of sample 2 (500 μm^2). Samples 4 and 5 show XRD patterns and UV−vis spectra that are identical to those shown in Figures 2b and 5b.

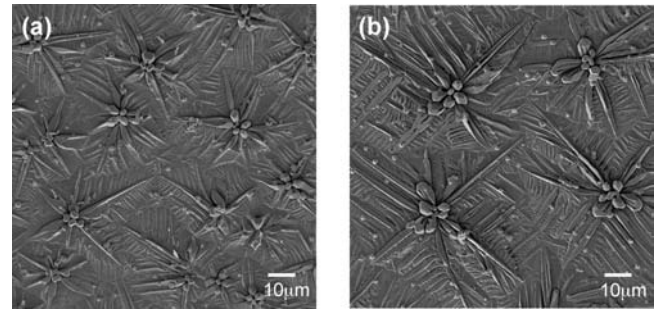

Figure 6. SEM of Cu_2O electrodes deposited using a buffered medium (pH 4.9) containing (a) 0.01 M $Cu(CH_3COO)_2$ (sample 4) and (b) 0.005 M $Cu(CH_3COO)_2$ (sample 5). The total concentration of acetic acid and acetate ion present in each solution were adjusted to be the same as that of the solution used to produce sample 2.

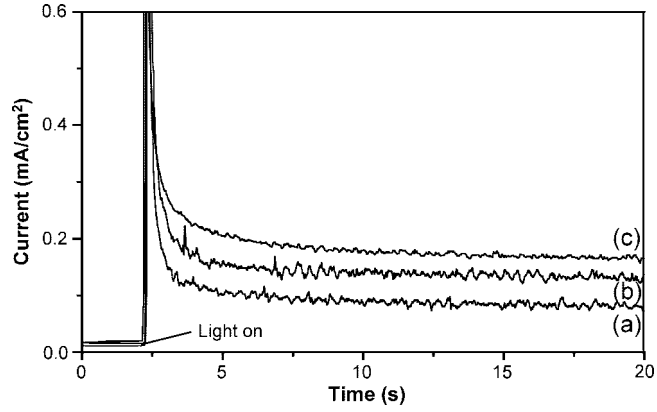

Figure 7. Zero-bias photocurrent of Cu_2O electrodes measured in a 0.02 M K_2SO_4 solution under 1 W/cm^2 illumination. Cu_2O electrodes were deposited using a buffered medium (pH 4.9) containing (a) 0.02 M $Cu(CH_3COO)_2$ (sample 2), (b) 0.01 M $Cu(CH_3COO)_2$ (sample 4), and (c) 0.005 M $Cu(CH_3COO)_2$ (sample 5).

Zero-bias photocurrents of samples 4 and 5 are shown in comparison with sample 2 in Figure 7. The steady-state photocurrent again increased as the crystal size increased. The steady-state photocurrent of sample 5 (0.16 mA/cm^2) is twice that of sample 2 (0.08 mA/cm^2). This is a substantial improvement considering that it is achieved simply by increasing dendritic crystal sizes without involving doping or band-gap tuning.

The third method we employed to vary the nucleation density involves altering the concentration of acetate ions used as buffer.

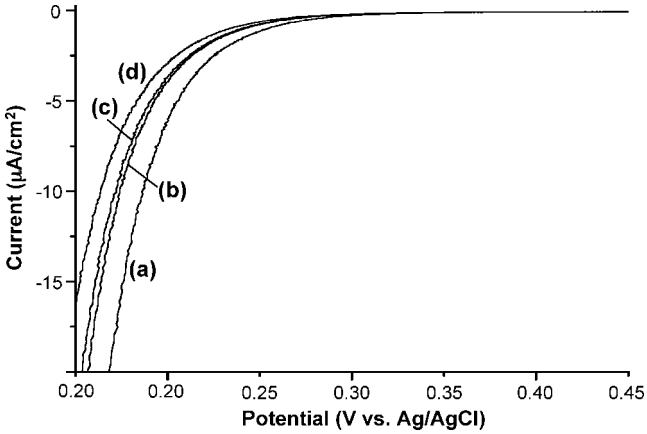

Figure 8. LSVs of a 0.02 M $Cu(CH_3COO)_2$ solution containing (a) 0.08, (b) 0.18, (c) 0.28, and (d) 0.38 M acetate buffer (pH 4.9). LSVs were recorded using a scan rate of 10 mV/s at 70 °C.

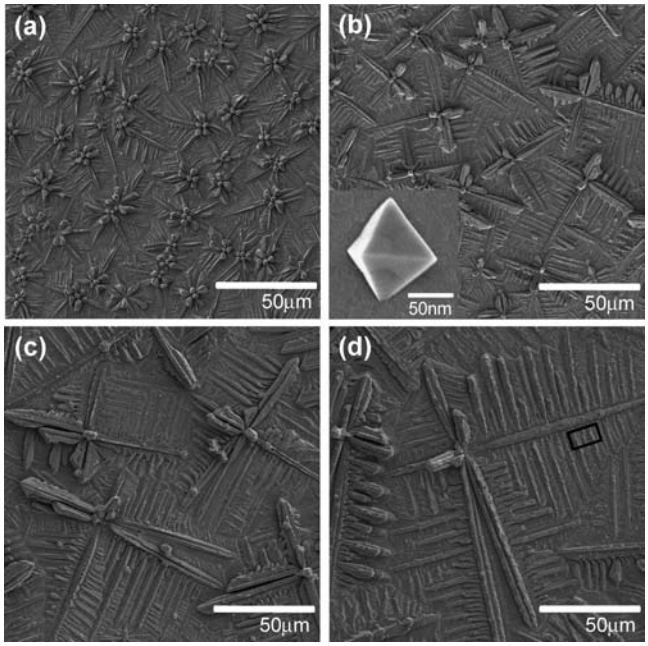

Figure 9. SEM images of Cu_2O electrodes deposited using a 0.02 M $Cu(CH_3COO)_2$ solution and (a) 0.08 (sample 2), (b) 0.18 (sample 6), (c) 0.28 (sample 7), and (d) 0.38 M (sample 8) acetate buffer (pH 4.9). The inset of b shows an SEM image of a dendritic crystal at an early stage. A high-magnification image of the boxed region in Figure 9d can be found in Figure 11a.

Acetate ions can act as complexing agents for Cu^{2+} ions and shift E_{red} of Cu^{2+} ions to the negative direction.[31] This effect can be visualized by linear sweep voltammetry (LSV) performed for Cu^{2+} reduction with varying concentrations of acetate buffer. Figure 8 shows that the onset potential to generate cathodic current by reduction of Cu^{2+} ions shifts gradually to the negative direction as the buffer concentration increases from 0.08 to 0.38 M. This means that when a fixed E_{appl} of 0.02 V is used for deposition, the electrode immersed in a medium with the most concentrated acetate ions will experience the least amount of η, resulting in a decrease in nucleation density.

Figure 9 shows SEM images of dendritic Cu_2O electrodes prepared from a 0.02 M $Cu(NO_3)_2$ solution containing 0.08 (sample 2), 0.18 (sample 6), 0.28 (sample 7), and 0.38 M (sample 8) acetate buffer. These images show that the acetate concentration indeed affects the nucleation density and that the crystal domain size increases as the concentration of acetate increases. Sample 8 contains the largest dendritic crystals branches of which extend longer than 100 μm. The average lateral size of crystals for samples 6, 7, and 8 are 2000, 4000, and 12000 μm^2, respectively.

It may be worthwhile to note that the general crystal shape in samples 6−8 is no longer truncated octahedral but octahedral. This is because the media used to prepare these samples contain more acetate ions that made growth along the ⟨111⟩ direction significantly slower than growth in the ⟨100⟩ direction. As a result, only {111} planes remained in the final shape, forming an octahedral shape. The inset of Figure 9b shows a representative SEM image of a crystal at an early stage of dendritic branching growth in samples 6−8.

The zero-bias photocurrent of these electrodes once again shows the same trend: photocurrent increases as the crystal size increases (Figure 10). Reproducing the same relationships between the crystal size and photocurrent using three different methods to alter the crystal size confirms that the changes in photocurrent are truly caused by altering the crystal domain size. The photocurrent enhancement observed by sample 8 is quite intriguing in that its photocurrent (0.45 mA/cm^2) is more than 20 times higher than that of sample 1 (0.02 mA/cm^2), which

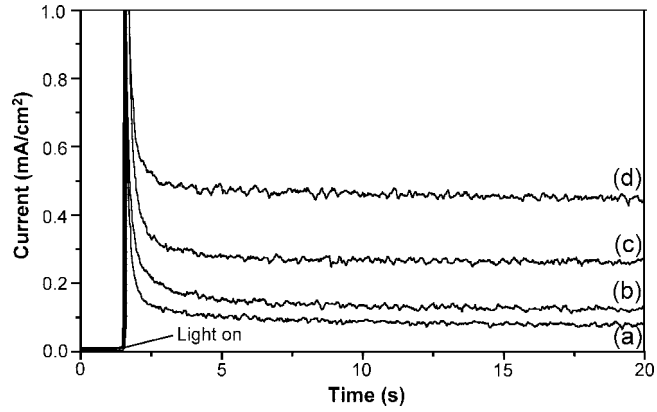

Figure 10. Zero-bias photocurrent of Cu_2O electrodes measured in a 0.02 M K_2SO_4 solution under 1 W/cm^2 illumination. Cu_2O electrodes were deposited using a 0.02 M $Cu(CH_3COO)_2$ solution containing (a) 0.08, (b) 0.18, (c) 0.28, and (d) 0.38 M acetate buffer (pH 4.9).

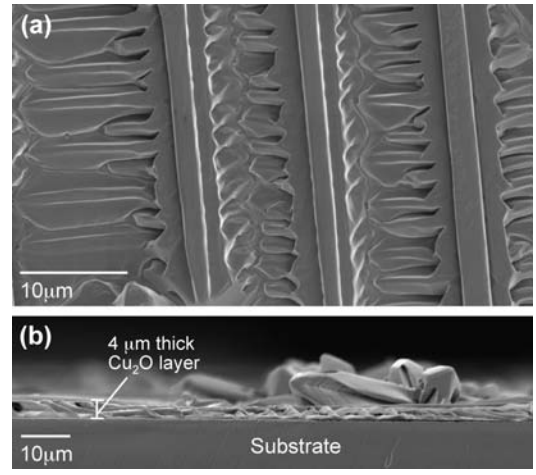

Figure 11. (a) Front-view and (b) side-view SEM images of sample 8.

(31) Pletcher, D.; Walsh, F. C. *Industrial electrochemistry*, 2nd ed.; Chapman and Hall: New York, 1990; p 403.

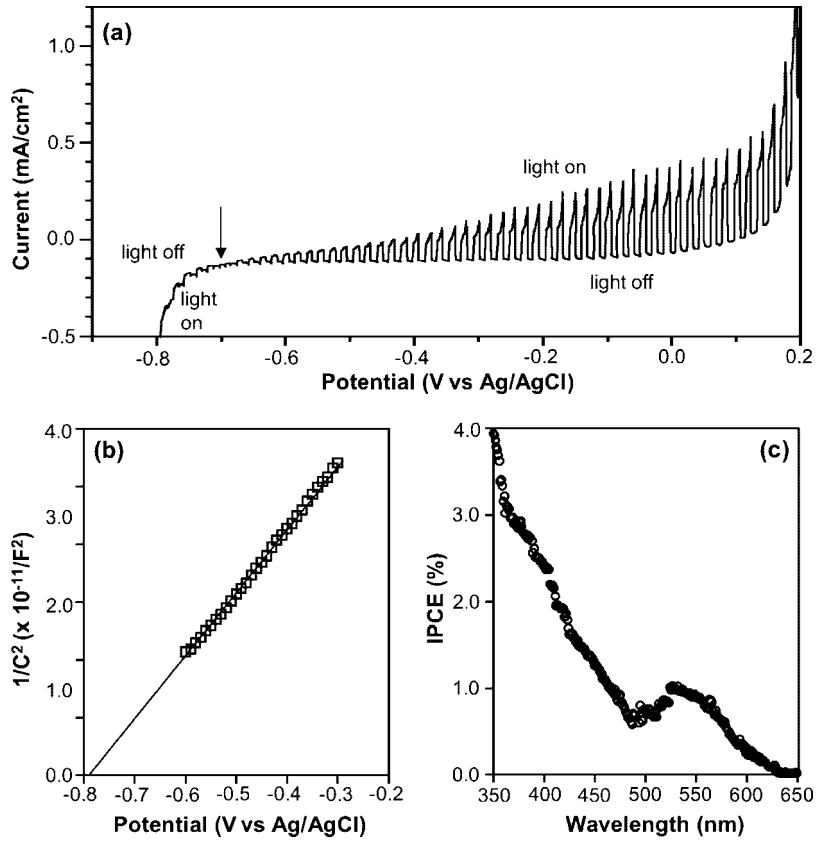

Figure 12. (a) LSV measured with chopped light (100 mW/cm^2, 1 Hz), (b) Mott−Schottky plot measured at 10 kHz, and (c) photocurrent action spectrum of sample 8. A 0.2 M K_2SO_4 solution was used as the electrolyte for these measurements. The arrow in Figure 12a shows the position where a transition from anodic photocurrent to cathodic photocurrent is observed.

has the smallest crystal domain size. The fact that this level of photocurrent enhancement can be achieved solely by tuning dendritic growth demonstrates the importance of methodical morphology control for constructing high-performance polycrystalline photoelectrodes.

Higher magnification SEM images of sample 8 show detailed morphological features of the sample responsible for the photocurrent enhancement (Figure 11). The front-view image shows the seamless, single-crystal-like nature of branches (Figure 11a), which ensures excellent electrical continuity within the dendritic crystals. This image also shows how the intricate side branching pattern, generated naturally without the need of templates, increases the micrometer-level surface roughness of the electrodes. Between the side branches grain boundaries do exist, but this grain boundary area is significantly lower than those present in the electrodes composed of typical nano- or micrometer-sized crystals/particles. The side-view images show that while the main branches on the substrate grow longer than 100 μm, the average film thickness remains below 5 μm except for the regions that contain branches growing of out the substrate (Figure 11b). These features combined together create a unique Cu_2O architecture that allows for high surface areas and good charge-transport properties.

Figure 12a shows LSV of sample 8 measured with chopped light (100 mW/cm^2, 1 Hz) in a 0.2 M K_2SO_4 solution. As the potential sweeps to the negative direction, the anodic photocurrent decreases because the band bending decreases and the rate of electron−hole recombination increases accordingly, which is a typical behavior of an n-type photoelectrode. The anodic photocurrent disappears around −0.7 V, and a small amount of cathodic photocurrent appeared before significant cathodic dark currents were generated. This anodic to cathodic photocurrent conversion provides a good indication that the flatband potential of sample 8 is located near −0.7 V.[32] A more accurate position of the flatband potential (U_{fb}) was obtained by taking the x intercept of the Mott−Schottky plot of sample 8 (Figure 12b), which gave $U_{fb} = -0.78$ V vs the reference electrode (equivalent to −0.58 V vs NHE). The positive slope of the plot again proved the n-type nature of our Cu_2O electrodes.

The photocurrent action spectrum for sample 8 measured without applying an external bias is shown in Figure 12c. The photocurrent onset was observed at $\lambda = 630$ nm, which is equivalent to the band gap of the material. The low IPCE in the visible region (∼1%) suggests that the carrier density in the Cu_2O layer and the interfacial kinetics at the Cu_2O/electrolyte interface need to be improved significantly. We also observed anodic photocorrosion when the Cu_2O electrode was illuminated with intense light for an extended period. Decreasing resistivity and increasing interfacial hole transfer kinetics of the Cu_2O electrodes will also be beneficial for kinetically suppressing photocorrosion. We are currently working on doping, surface treatment (e.g., catalyst deposition, surface modification), and further optimization of morphology of the Cu_2O electrodes, which will create various opportunities to build Cu_2O-based photoelectrochemical and photovoltaic devices.[2,33−35]

Conclusions

We demonstrated a new strategy of exploiting and manipulating dendritic growth of Cu_2O to produce photoelectrodes with

(32) Dare-Edwards, M. P.; Goodenough, J. B.; Hamnett, A.; Trevellick, P. R. *J. Chem. Soc., Faraday Trans.* **1983**, *79*, 2027–2040.

high surface areas and good electrical continuity. Dendritic growth of Cu_2O was stabilized by employing buffered media to prevent the local pH drop at the working electrode that promotes faceted growth. The dendritic branching growth of Cu_2O allowed for facile substrate coverage and high surface areas without growing a thick film. The resulting electrodes generated significantly improved anodic photocurrent (n-type behavior) compared to the electrodes composed of micrometer-sized faceted crystals that produced negligible zero-bias photocurrent. In order to further enhance photocurrent, various methods to increase dendritic crystal size were investigated. Increasing crystal size reduces crystal−crystal boundary areas and ensures good electrical continuity in the larger domains of the electrode. This can minimize recombination losses and improve charge-transport properties. Deposition potential, Cu^{2+} concentration, and acetate concentration were altered to regulate the deposition overpotential, η, which has a direct impact on nucleation density and, therefore, crystal size. Increasing crystal size consistently resulted in the improvement of photocurrent regardless of the method used to regulate crystal size. The electrode showing the highest photocurrent was composed of dendritic crystals that laterally expanded ca. 12000 μm^2 while the thickness of the electrode was kept below 5 μm. This electrode (sample 8) generated more than 20 times higher photocurrent than the electrode containing the smallest crystal size produced in this study with an average lateral size of 100 μm^2 (sample 1). The significant increase in photocurrent achieved simply by controlling the crystal sizes in dendritic branching growth, without involving any compositional changes, implies an enormous potential for morphology tailoring in improving the properties of polycrystalline electrodes.

LSV using chopped light and the Mott−Schottky plot of sample 8 confirmed its n-type nature and provided the position of the flatband potential (−0.78 vs reference electrode in pH 6 solution). The IPCE measured without applying an external bias is approximately 1% for the visible region. This suggests that improvements are necessary in charge-transport processes and interfacial kinetics through composition tuning (e.g., doping, catalysts deposition, surface treatment) as well as further morphology optimization of n-type Cu_2O electrodes. These studies will enable us to construct various homo- and heterojunction photoelectrodes based on Cu_2O for efficient visible light conversion.

Acknowledgment. This work was supported by the U.S. Department of Energy (DE-FG02-05ER15752), the Alfred P. Sloan foundation, and the donors of the American Chemical Society Petroleum Research Fund. It made use of the Life Science Microscopy Facility at Purdue University. The authors thank Ryan Spray and Drs. Craig Grimes, Karthik Shankar, Hugh Hillhouse, and Manoj Namboothiry for their help in measuring photocurrent action spectra.

Supporting Information Available: Zero-bias photocurrent and SEM image of p-type Cu_2O electrodes electrodeposited using an alkaline plating solution (pH 11). This material is available free of charge via the Internet at http://pubs.acs.org.

JA806370S

(33) Martinez-Ruiz, A.; Moreno, M. G.; Takeuchi, N. *Solid State Sci.* **2003**, *5*, 291–295.
(34) Ishizuka, S.; Kato, S.; Okamoto, Y.; Sakurai, T.; Akimoto, K.; Fujiwara, N.; Kobayashi, H. *Appl. Surf. Sci.* **2003**, *216*, 94–97.
(35) Okamoto, Y.; Ishizuka, S.; Kato, S.; Sakurai, T.; Fujiwara, N.; Kobayashi, H.; Akimoto, K. *Appl. Phys. Lett.* **2003**, *82*, 1060–1062.